Superposed epoch analysis of magnetotail flux transport during substorms observed by THEMIS

J. Liu,[1] C. Gabrielse,[1] V. Angelopoulos,[1] N. A. Frissell,[2] L. R. Lyons,[3] J. P. McFadden,[4] J. Bonnell,[4] and K. H. Glassmeier[5,6]

Received 30 June 2010; revised 11 October 2010; accepted 8 December 2010; published 15 March 2011.

[1] Cumulative magnetic flux transport earthward/tailward of the reconnection site in the plasma sheet or equatorward toward the neutral sheet (Φ) has been shown to be one of the most useful quantities for remotely sensing reconnection onset in the magnetotail. We examine the behavior of Φ during substorms near the onset meridian using superposed epoch analysis of Time History of Events and Macroscale Interactions during Substorms (THEMIS) probe observations at different downtail distances. Observational data come from the THEMIS Substorm Database, assembled under the auspices of the Geospace Environment Modeling (GEM) program (http://www.igpp.ucla.edu/themis/events/). We find that Φ starts to increase a few minutes prior to ground midlatitude Pi2 onset. Although our study cannot monitor regions beyond 30 R_E, the apogee of the most distant probe (P1), enhanced transport tends to begin at 20–30 R_E and moves progressively inward just prior to ground Pi2 onset. Our results are consistent with recent THEMIS case studies showing that reconnection initiates the substorm expansion phase process.

Citation: Liu, J., C. Gabrielse, V. Angelopoulos, N. A. Frissell, L. R. Lyons, J. P. McFadden, J. Bonnell, and K. H. Glassmeier (2011), Superposed epoch analysis of magnetotail flux transport during substorms observed by THEMIS, *J. Geophys. Res.*, *116*, A00I29, doi:10.1029/2010JA015886.

1. Introduction

[2] Substorms are global reconfigurations of the magnetosphere involving solar wind energy storage in Earth's magnetotail and abrupt conversion of energy to particle heating and kinetic energy [*Akasofu*, 1964; *Axford*, 1999]. Substorms are responsible for various well-documented magnetotail and ground phenomena associated with magnetic reconnection in the tail.

[3] The most defining aspect of a substorm, auroral intensification and poleward expansion [*Akasofu*, 1964], is caused by closure of intense, field-aligned currents in the ionosphere. According to recent evidence, the initial intensification may be related to wave-accelerated electrons [*Mende et al.*, 2003] rather than monoenergetic electrons caused by "inverted-V" type, field-aligned potential drops. Rapid auroral intensification, breakup of auroral forms into smaller filaments, poleward expansion, and westward surge of the most intense auroral arcs are the ground signatures of auroral substorms. *Nishimura et al.* [2010] showed that a few minutes prior to substorm auroral intensification onset (as defined by *Akasofu* [1964]), poleward boundary intensifications (PBIs) observed at high latitudes produce north-south (N-S) arcs. In a matter of minutes, these arcs propagate equatorward along ionospheric convection streamlines [*Lyons et al.*, 2010a] and reach the ionospheric location of substorm auroral intensification at the time of onset. Since PBIs are expected to result from tail reconnection that has reached the open-closed flux boundary [*Sergeev et al.*, 2000], and N-S arcs map to earthward flows [*Zesta et al.*, 2000], the auroral sequence of *Nishimura et al.* [2010] suggests that lobe reconnection should start on average ~5.5 min prior to auroral intensification or poleward expansion. On the other hand, *Kepko et al.* [2009] posits that N-S arcs only 1–2 degrees poleward of the substorm arc may start deep within closed plasma sheet field lines only 2 min prior to onset. The event studied by *Kepko et al.* [2009] may be one of a subset of substorms in which reconnection starts and remains within closed field lines, i.e., closer to Earth than open field line reconnection. Further work is needed to identify the radial distance at which lobe reconnection typically starts and the time delay of that process relative to substorm auroral intensification onset.

[4] The currents responsible for the auroral forms also produce ground magnetic signatures, including an abrupt increase in the auroral electrojet (AE) index and irregular magnetic field pulsations in the 40–150 s range called Pi2 pulsations [*Jacobs et al.*, 1964; *Saito*, 1969]. Pi2 pulsations are excited at the foot point of the substorm current wedge

[1]IGPP, ESS, University of California, Los Angeles, California, USA.
[2]Bradley Department of Electrical and Computer Engineering, Virginia Polytechnic Institute and State University, Blacksburg, Virginia, USA.
[3]Department of Atmospheric and Oceanic Sciences, University of California, Los Angeles, California, USA.
[4]Space Sciences Laboratory, University of California, Berkeley, California, USA.
[5]Technische Universität Braunschweig, Braunschweig, Germany.
[6]Max Planck Institute for Solar System Science, Katlenburg-Lindau, Germany.

0148-0227/11/2010JA015886

(high-latitude Pi2s) and then propagate equatorward to midlatitude [*Kepko et al.*, 2002]. According to *Kepko et al.* [2002], midlatitude Pi2s are caused by structured incoming flows. Other authors [*Takahashi et al.*, 2003; *Allan et al.*, 1996; *Baumjohann and Glassmeier*, 1984], however, suggest they may be due to the excitation of a cavity mode resonance or field-aligned currents from the substorm current wedge. There may indeed be multiple ways of exciting such waves at various latitudes. In any case it has been established [*Liou et al.*, 2000] that at least for Pi2-associated auroral intensifications, midlatitude Pi2s are observed within 1–2 min after auroral intensification onsets. Unlike high-latitude Pi2s, which are only observed near the foot point of a substorm current wedge, midlatitude Pi2s are observed consistently at ground stations and thus are a good indicator of substorm onset even when ground or space imagers are not available.

[5] In the magnetotail, the substorm current wedge system [*McPherron*, 1979] and local magnetic field dipolarizations [*Lopez and Lui*, 1990] are observed at 6–10 R_E, whereas earthward bursty bulk flows [*Angelopoulos et al.*, 1992, 1994] are found at 8–20 R_E. Further downtail, tailward moving plasmoids [*Hones*, 1980; *Slavin et al.*, 1984] and TCRs [*Slavin et al.*, 1984] have been observed in association with substorms; these plasmoids/TCRs are generated by reconnection near the Earth [*McPherron et al.*, 1973; *Hones*, 1980]. Flows accompanying reconnection are at a distance from the reconnection site when observed near the neutral sheet [*Hayakawa et al.*, 1982; *Nishida et al.*, 1981; *Hones*, 1980; *Nagai*, 2006]. Closer to the reconnection site, deflection of the tail field consistent with magnetic reconnection topology (X line or X point) is expected, i.e., a northward deflection of the field earthward of the reconnection site, and a southward deflection on the tailward side of the reconnection site. Thus, earthward/tailward flows threaded by northward/southward fields are the classical definition of reconnection, as viewed near the neutral sheet.

[6] During substorms, however, the current sheet is very thin and satellites often make observations at a large distance (comparable to the current sheet scale size) from the neutral sheet. This makes the classical signature of reconnection hard to capture. *Angelopoulos et al.* [2009] showed that, as predicted by reconnection topology, the observation of inward flows toward the reconnection point is a reasonable definition of reconnection onset when probes are making observations at the plasma sheet boundary layer. They found that the onset of equatorward flows toward the neutral sheet is well determined by an abrupt increase in cumulative magnetic flux transport toward the neutral sheet (calculated as the cumulative integral of the dawn-dusk component of the electric field), and this abrupt onset of flux transport can serve well as an indicator for the timing of reconnection onset.

[7] Other recent studies have demonstrated the association between magnetic flux transport and not only inward flow toward the neutral sheet, but also dipolarizations, presumably caused by reconnection outflows [*Liu et al.*, 2009, 2011]. The integral of E_y (hereafter referred to as Φ) represents cumulative magnetic flux transport earthward and tailward out of the reconnection site or equatorward toward the reconnection site from the lobe. Very close to the reconnection site, positive E_y and a sharp increase in Φ are expected when reconnection is turned on, even when the satellite is near the plasma sheet boundary layer, due to the continuous cross-tail electric field across the reconnection region. Given the extreme thinning of the plasma sheet during the late growth phase, we expect the aforementioned cumulative integral to be a reliable indicator of plasma sheet or lobe reconnection onset, as well as reconnection outflow arrival in the near-Earth region.

[8] However, if the probe is a great distance downstream of the X line (on the tailward side of a plasmoid/flux rope or the earthward side of an earthward moving flux rope), it will observe lobeward-then-inward plasma motion and a negative-then-positive E_y (constant flow, bipolar B_z) in the plasma sheet. Thus at times Φ will be observed to be first decreasing and then increasing even after the onset of tail reconnection, depending upon the satellite location. In summary, satellites in the tail will observe an abrupt increase in Φ immediately after reconnection onset most of the time. Unlike signatures that can only be captured in a narrow band very close to the neutral sheet, such as bursty bulk flows, an abrupt increase in cumulative magnetic flux transport can be observed even when the satellites are near the plasma sheet boundary layer.

[9] The goal of this work is to determine statistically whether there is a systematic increase in cumulative magnetic flux transport into the tail providing evidence of reconnection, and the onset time of this increase at different tail locations relative to ground substorm onset. We use midlatitude Pi2s to determine ground onset time to within 1–2 min because unlike high-latitude Pi2s, midlatitude Pi2s are a global indicator of onset and are unaffected by cloudiness, which limits the use of auroral optical stations. Studies of the first signatures of a substorm in the midtail by *Miyashita et al.* [2009] concluded that pressure reduction at the 16–20 R_E downtail region is the first indicator of reconnection onset (~2 min prior to ground onset), based on a large substorm database from the Geotail mission. *Miyashita et al.* [2009] did not examine the flux transport criterion because it had not yet been recognized as an excellent indicator of reconnection onset.

[10] The Time History of Events and Macroscale Interactions during Substorms (THEMIS) mission [*Angelopoulos et al.*, 2008a; *Sibeck and Angelopoulos*, 2008] provides a useful multi-instrument, multiprobe database for our study of cumulative magnetic flux transport. High-sensitivity electric field, magnetic field, and plasma instruments on five THEMIS probes distributed along the tail [*Bonnell et al.*, 2008; *McFadden et al.*, 2008] produce a statistical ensemble of flux transport data from multiple distances for the same geomagnetic conditions. A network of ground-based observatories (GBOs) is deployed to determine the meridian and onset time of Pi2 pulsations and auroral intensification [*Mann et al.*, 2008; *Mende et al.*, 2008; *Russell et al.*, 2008]. THEMIS has proved its power in case studies of substorm timing [e.g., *Angelopoulos et al.*, 2008b; *Gabrielse et al.*, 2009; *Liu et al.*, 2009; *Pu et al.*, 2010], and its potential in statistical studies has been recognized (T.-S. Hsu, A statistical analysis of the effects of fast plasma flows on the Pi2 pulsations, manuscript in preparation, 2011). Following three substorm observations by *Angelopoulos et al.* [2009] and 13 substorm studies by *Lyons et al.* [2010b], we study the flux transport criterion statistically using the THEMIS

Substorm Timing Table (http://www.igpp.ucla.edu/themis/events/) [*Gabrielse et al.*, 2010]. A subset of substorms from this table that were observed in the tail within the substorm meridian is used.

[11] Following the introduction of our instrumentation and database, we explain the anticipated pattern of cumulative flux transport Φ during substorms and introduce the raw data processing method. We then report on the results of our superposed epoch analysis and conclude with a discussion.

2. Instrumentation and Database

[12] THEMIS, launched on 17 February 2007, consists of five identical probes equipped with comprehensive particle and field instruments. During the first two years of operation, the probes were aligned along the Sun-Earth line in the magnetotail plasma sheet to determine the onset mechanism of substorms by timing propagation delays between different points in the magnetosphere and the ionosphere [*Angelopoulos*, 2008]. They traversed the magnetotail with different apogees [*Sibeck and Angelopoulos*, 2008]: Probe 1 (P1), ~30 R_E; P2, ~20 R_E; P3 and P4, ~12 R_E; and P5, ~10 R_E. (Note that the probe names are given both in letters and numbers: TH-B, C, D, E, and A corresponding to P-1, 2, 3, 4, and 5; i.e., the letter sequence matches the number sequence after cyclical permutation by one letter position). Probe apogees and active control of in-orbit phasing enable observations of the same event in alignment at various altitudes. Alignments are timed to be between 00 and 12 UT, when the North American continent is over the nightside. Twenty THEMIS ground-based observatories (GBOs) [*Mende et al.*, 2008], deployed from eastern Canada to western Alaska (several being part of CARISMA (http://www.carisma.ca [*Mann et al.*, 2008]) and GIMA (http://magnet.gi.alaska.edu/) magnetometer arrays) provide all-sky aurora images and ground magnetic field data. An additional 11 Education and Public Outreach (EPO) magnetometers [*Russell et al.*, 2008] deployed across the United States complement the ground magnetometer array with subauroral and midlatitude observations. These observatories help determine the time of auroral intensification onset, negative bays, and ULF wave onset.

[13] Observations from December 2007 to April 2008 constitute the first tail season for THEMIS alignments. During that period the outer probes (P1, P2) remained at a nominal distance from the neutral sheet (<5 R_E) to determine the onset of particle acceleration in the midtail from plasma sheet boundary layer beams or currents. In retrospect, the signatures of plasma sheet boundary beams and flows observed by the outer probes were scarcely near onset, while bipolar fields (TCRs/NFTEs) dominated the midtail signatures of onset. This was attributed to extreme plasma sheet thinning during substorm onset. For the second tail season (December 2008 to May 2009), the orbits of P1 and P2 were changed to be within 2 R_E from the neutral sheet. This yielded substorm observations from close proximity to the neutral sheet comparable in number to those in the first year, despite reduced solar activity (due to a prolonged solar minimum) during the second tail season.

[14] The substorms used herein are listed in the THEMIS Substorm Timing Table (http://www.igpp.ucla.edu/themis/events/) [*Gabrielse et al.*, 2010], which contains 46 events during THEMIS major conjunctions (all five probes are aligned along the Sun-Earth line) and 40 events during THEMIS minor conjunctions (P2–5 are aligned along the Sun-Earth line) for the 2007–2008 tail season. It also contains 16 major conjunction events and 22 minor conjunction events for the 2009 tail season. Approximately 80 different parameter values, either calculated or measured directly at the five THEMIS probes, the GBOs or the EPO magnetometers, were assigned to each event. These parameters characterize the event onset time at various locations, the geometry of the conjunction, the location and extent of auroral breakup, the potential signature of reconnection onset, current disruption, and the intensity of presubstorm convection and auroral activity. Each parameter was determined by a different expert to form a consistent onset determination across multiple events and also to provide a more unbiased determination of the time sequence of events before and during onset.

[15] In the following we calculate the cumulative magnetic flux transport using magnetic field measurements from the Fluxgate Magnetometer (FGM) [*Auster et al.*, 2008], ion bulk velocity measurements from the Electro-Static Analyzer (ESA) [*McFadden et al.*, 2008], and electric field data from the Electric Field Instrument (EFI) [*Bonnell et al.*, 2008] on the THEMIS probes. We also use GBO and EPO magnetometer data to determine the ground high-latitude and midlatitude Pi2 onset times of the substorm events.

3. Calculation of the Cumulative Magnetic Flux Transport and Its Role as a Reconnection Identifier

[16] The inflection point of the cumulative magnetic flux transported earthward/tailward and toward the neutral sheet per unit length in the Y_{GSM} direction observed by probes in the tail has been used as an identifier of reconnection onset [*Angelopoulos et al.*, 2009; *Liu et al.*, 2009, 2011]. It is calculated by

$$\Phi = -\int (v_x B_z - v_z B_x) dt, \tag{1}$$

where v_x and v_z are the x and z components of the ion bulk velocity, and B_x and B_z are the x and z components of the magnetic field (all in GSM coordinates). B_x is positive northward of the neutral sheet and negative southward of it. Thus, the term $-v_z B_x$ means the magnetic flux transferred toward the neutral sheet per unit length in the Y_{GSM} direction per unit time. During a reconnection event, B_z is positive earthward of the reconnection site and negative tailward of the reconnection site. Therefore, the term $v_x B_z$ denotes the magnetic flux transferred earthward per unit length in the Y direction per unit time if the probe is earthward of the reconnection site, or the magnetic flux transferred tailward per unit length in the Y direction per unit time if the probe is tailward of the reconnection site, in the absence of a flux rope. The flux transport can also be calculated with $\Phi = \int E_y dt$ where E_y is the y component of the electric field in GSM coordinates, since $\mathbf{E} = -\mathbf{v} \times \mathbf{B}$, and the ion and electron gradient drifts are predominantly in the Y direction and do not affect the computation of E_y. Earthward of 7 R_E, the azimuthal flow due to pressure gradients is as important as the earthward flow [e.g.,

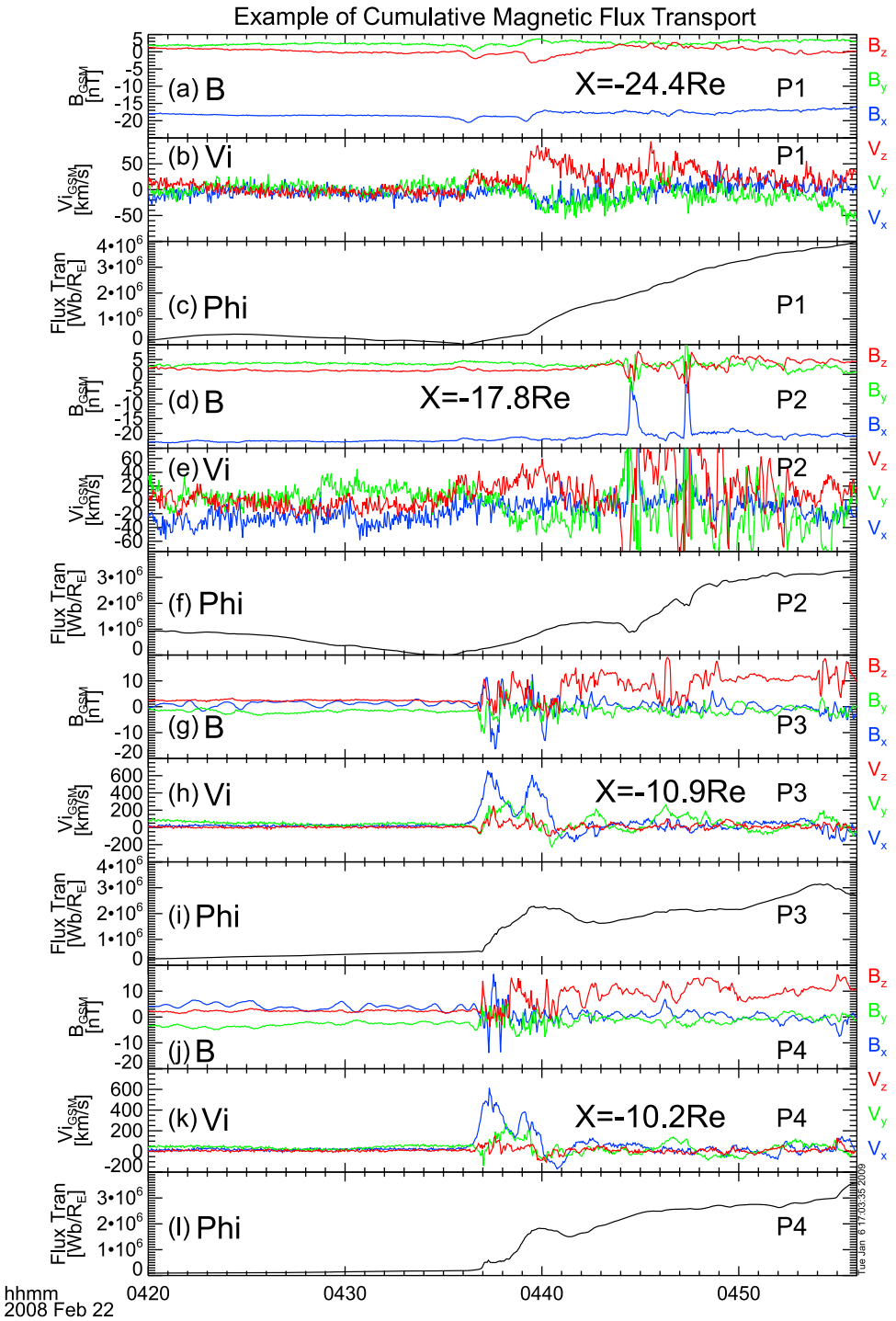

Figure 1. An example of the cumulative magnetic flux behaviors during the 22 February 2008 substorm event [*Liu et al.*, 2009]. For each probe, we show magnetic field in GSM coordinates, low-energy (ESA) ion bulk velocity, and cumulative magnetic flux transferred earthward/tailward and into the plasma sheet per unit time per unit length (calculated from the integration of the y component of $-\mathbf{Vi_{GSM}} \times \mathbf{B_{GSM}}$ over time). Please see *Liu et al.* [2009] for satellite positions and other details of this event.

Angelopoulos et al., 1993], so the flux transport is calculated as $\Phi = \int E_r dt$ in this condition, where E_r is the radial component of the electric field in spherical coordinates in GSM coordinates.

[17] According to the near-Earth neutral line model, the plasma sheet continues to thin during the growth phase of a substorm. The tail lobe flux, however, increases due to loading from the solar wind, producing an inductive electric

Table 1. The Substorm Events Used in the Superposed Epoch Analysis Ordered by Their Ground Pi2 Onset Time[a]

Event Pi2 Onset	Event	Event Pi2 Onset	Event
2007-12-28/0058:10	1	2008-02-28/0157:44	47
2007-12-28/0426:06	2	2008-02-28/0344:20	48
2008-01-01/0346:00	3	2008-02-28/0752:34	49
2008-01-03/0732:40	4	2008-02-28/1110:18	50
2008-01-03/0820:30	5	2008-03-01/0149:08	51
2008-01-05/0758:18	6	2008-03-01/0357:24	52
2008-01-07/0030:54	7	2008-03-05/0200:52	53
2008-01-07/0448:38	8	2008-03-05/0639:24	54
2008-01-07/1044:12	9	2008-03-11/0553:52	55
2008-01-13/0332:50	10	2008-03-13/1105:58	56
2008-01-13/0514:58	11	2008-03-17/1022:30	57
2008-01-15/0135:30	12	2008-03-21/0717:22	58
2008-01-15/0949:34	13	2008-03-23/0107:34	59
2008-01-15/1119:10	14	2008-03-27/0230:10	60
2008-01-17/0012:42	15	2009-01-26/0741:28	61
2008-01-17/0642:44	16	2009-02-01/0956:30	62
2008-01-19/0610:14	17	2009-02-05/0745:20	63
2008-01-19/1002:10	18	2009-02-07/0355:28	64
2008-01-21/0405:48	19	2009-02-09/0734:24	65
2008-01-21/0713:08	20	2009-02-11/0745:04	66
2008-01-23/0609:34	21	2009-02-15/0323:34	67
2008-01-25/0841:16	22	2009-02-15/1129:32	68
2008-01-27/0224:10	23	2009-02-17/0717:22	69
2008-01-29/0743:58	24	2009-02-19/1006:52	70
2008-02-02/0337:36	25	2009-02-21/0937:14	71
2008-02-02/0740:54	26	2009-02-23/0835:04	72
2008-02-04/0058:34	27	2009-02-25/0857:12	73
2008-02-04/0842:28	28	2009-02-27/0224:30	74
2008-02-08/0407:18	29	2009-02-27/0822:22	75
2008-02-10/0442:48	30	2009-03-01/0807:48	76
2008-02-12/0254:16	31	2009-03-05/0304:50	77
2008-02-12/0626:10	32	2009-03-05/0809:34	78
2008-02-12/0627:18	33	2009-03-09/0605:20	79
2008-02-14/0233:58	34	2009-03-09/0907:44	80
2008-02-14/1158:04	35	2009-03-13/0529:50	81
2008-02-16/0244:52	36	2009-03-13/1111:50	82
2008-02-16/0730:08	37	2009-03-15/0212:58	83
2008-02-18/0353:20	38	2009-03-15/0429:44	84
2008-02-18/0943:12	39	2009-03-15/0805:30	85
2008-02-20/0330:12	40	2009-03-17/0548:24	86
2008-02-20/0705:06	41	2009-03-19/0653:52	87
2008-02-22/0437:54	42	2009-03-23/0603:32	88
2008-02-22/0904:26	43	2009-03-25/0203:20	89
2008-02-26/0406:42	44	2009-03-25/0857:46	90
2008-02-26/0454:08	45	2009-03-29/0513:36	91
2008-02-26/0957:46	46		

[a]Each event is marked by an event number to its right.

field that opposes the convective electric field [*Pritchett and Coroniti*, 1995]. The net result is a limited flow into (or out of) the plasma sheet and a very small net cumulative flux transport toward or away from the neutral sheet, depending on the efficacy of the inductive field in opposing the nominal convection. At reconnection onset, the magnetic flux is transported rapidly earthward and tailward with the outflow within the plasma sheet; an equivalent amount of transport per unit cross-tail length is expected from the lobes into the plasma sheet. Thus, regardless of its location (plasma sheet or boundary layer) surrounding the reconnection point, the electric field is primarily in the Y direction, and the cumulative flux transport of (1) is positive. Farther away from the neutral point (either earthward or tailward), however, a bipolar signature of a flux rope may be evident ahead of the classical in/outflow. The flux rope may result in a bipolar magnetic and electric field signature prior to the nominal X point, making the cumulative flux transport slightly decreases before it increases. In summary, slow evolution of the integrated tail flux transport is expected before reconnection onset and a sudden increase in flux transport should be observed at reconnection onset (or slightly thereafter if the observation point is far away from the X point such that a flux rope precedes the X line signature).

[18] Figure 1 shows an example of cumulative flux transport behavior at various distances during the ~0430 UT, 22 February 2008 substorm [*Liu et al.*, 2009]. In that event reconnection onset was determined to be at 0434:25~0435:04 UT at X_{GSM} = −19.5 ~ −22.4 R_E. As the reconnection-generated plasma arrived at the inner edge of the plasma sheet where P3 and P4 were situated, these probes observed an increase in cumulative flux transport (Figures 1i and 1l). On the other side of the X point, P1 and P2 also observed sudden increases in the flux transport after reconnection onset, simultaneous with plasmoid/NFTE passage/magnetic field deflection. The flux transport, however, decreased before the onset time instead of undergoing a slow increase (Figures 1c and 1f). Most of the transport is due to the Z-directed inflow to the plasma sheet, consistent with inflow to the reconnection site. Such patterns are also found in other substorm events such as that studied by *Angelopoulos et al.* [2009] and *Lyons et al.* [2010b]. Thus, although probes may be occasionally too far from the neutral sheet to observe the earthward/tailward flows, presumably due to the thinness of the reconnection geometry in the north-south direction, the continuity of the reconnection electric field throughout the active region makes flux transport Φ a good indicator of reconnection.

4. Superposed Epoch Analysis: Methods

[19] We examine the generality of the observable Φ as a reconnection onset identifier during substorms, using a superposed epoch analysis of observations made during the substorm events in the THEMIS Substorm Timing Table. Only events with isolated ground Pi2 onset timing are considered. We use midlatitude Pi2 onset times as a proxy for substorm onset time because they can be well determined for most of the substorm events and because they are global, i.e., their timing is clear and not predicated on ground stations which are within the substorm meridian. When defined as power increase above a threshold, midlatitude Pi2 onsets are observed on average within 1–2 min after auroral intensification onsets [*Liou et al.*, 2000]. Even though improved definitions [*Kepko and McPherron*, 2001] can reduce that error, we expect our visual selection of Pi2 onset from the inflection point of Pi2 power to be subject to such delay, if for no other reason than because the Pi2 wave period is comparable to that uncertainty. We hereafter use the term "Pi2 onset" to refer to the midlatitude ground Pi2 onset. We list all 91 events used in Table 1, organized by their Pi2 onset. For each event we use measurements from all five probes (whenever possible) and divide the observations into four groups based on where they were made. The four groups are as follows: Group A, probe position within 7 R_E downtail (in GSM) and outside the plasmasphere, i.e., ion density less than 10 per cc); Group B,

$-13\ R_E < X_{GSM} < -7\ R_E$; Group C, $-18\ R_E < X_{GSM} < -13\ R_E$; and Group D, $-30\ R_E < X_{GSM} < -18\ R_E$.

[20] We restrict our observations to within the premidnight sector of the magnetotail ($0 < Y_{GSM} < 8\ R_E$) since most substorm-related signatures occur in this region [*Nagai et al.*, 1998, 2005]. Because of the orbit of the THEMIS probes, Groups A and B observations are generally closer to the neutral sheet than those of Groups C and D, especially for first tail season observations (60% of the events included in our study).

[21] For each probe measurement, two methods are used to obtain E_y or E_r. One is to obtain the electric field data directly from the EFI. The EFI data are in DSL coordinates with Z along the spin axis [see *Angelopoulos*, 2008], so a coordinate transformation is needed to get E_{yGSM}. However, with its long wire booms, EFI can only measure the spin plane component of the DC electric field at high accuracy (<1 mV/m), whereas the shorter axial stacer booms can typically provide high-sensitivity AC information. Thus, the z component of the quasi-DC axial component of the electric field must be inferred from the two spin-plane components. We use the relationship $\mathbf{B} \cdot \mathbf{E} = 0$ (the parallel electric field is zero for low-frequency waves) to calculate $E_{z,DSL}$:

$$E_z = -\frac{E_x B_x + E_y B_y}{B_z}.$$

To prevent unrealistically large, noisy E_z values resulting from even small noise levels in B_z, we restrict the ratio between B_z and the magnetic field component in the X-Y plane to greater than tan(5°). E_z points where the magnetic field measurement does not meet this criterion are set to be "not a number" (NaN) values (E_x and E_y are also set to be NaN at these points), while the rest of the points are rotated to GSM using standard methods. For nearly taillike fields this treatment can lead to many indeterminate points in $\boldsymbol{E_{GSM}}$ and uncertainties in the computed cumulative magnetic flux transport. However, in most cases the duskward directed electric field is nearly identical in the two systems (DSL and GSM), except for a sign change to account for the spin axis of P1 and P2, which were close to ecliptic normal south. In other words, the spin planes of all probes were approximately in the X-Y_{GSM} plane, and the intersection of the spin plane and the X-Y_{GSM} plane lies very near the Y_{GSM} and Y_{DSL} axis, the direction of interest for this study. We surveyed THEMIS probe attitudes during all the substorms in Table 1 and found that in ~60% of the measurements, the angle between the Y_{DSL} ($-Y_{DSL}$ for P1 and P2) and Y_{GSM} axes was less than 20°; ~30% of the time the angle was between 20° to 30°; and the difference angle never exceeded 39°. Therefore, for Groups B–D we use $\pm E_{yDSL}$ to approximate E_{yGSM}. For Group A, which involves E_r (in the spherical coordinate system transformed from GSM), calculation of $\boldsymbol{E_{GSM}}$ is necessary, yet close to Earth the angle of the magnetic field to the spin plane is typically larger, and therefore application of the $\mathbf{E} \cdot \mathbf{B} = 0$ approximation rarely breaks down. Therefore, only a few data gaps in the superposed epoch analysis results of Group A are expected.

[22] A second method of determining E_{yGSM} is to use the plasma approximation. From the measured magnetic field and the computed ion bulk velocity data from ESA instrument, we can calculate the electric field as $E_{GSM} = -v_{iGSM} B_{GSM}$. For our superposed epoch analysis, we used the cumulative magnetic flux transport Φ integrated from E_y obtained with both methods for Groups B–D. For Group A, however, the probes were so close to Earth that ESA measurements of ion bulk velocity are insufficient since the ion thermal speed is sufficiently large that contributions to the ion velocity from energies beyond the energy range of the ESA instrument (0–25 keV) were needed. Moreover, those energies are dominated by diamagnetic drifts of particles in strong magnetic and particle pressure gradients, and therefore the simple plasma approximation used earlier does not apply. Thus, we do not include the flow-derived Φ in Group A in this study.

[23] One issue with the electric field data from EFI is that it always has an offset of a few tenths to a few mV/m, depending on component and plasma conditions. When integrating raw EFI data to obtain Φ, this offset will result in a monotonic trend in Φ on top of the physical cumulative transport profile, suppressing the reconnection onset signature. We thus seek to remove this offset by subtracting the value of the quiet time electric field measured under similar conditions from the measured electric field data. For most measurements, the quiet time average (offset) is selected from the hour prior to the start of the electric field perturbation related to onset by choosing time periods when the field fluctuations were near zero. For several events during which the electric field was variable before Pi2 onset time, a quiet time right after the substorm was used to determine offset. For even fewer events during which the measured electric field was variable both before and after Pi2 onset time, the average of the least variable time range prior to Pi2 onset was used as the offset. When E_r was calculated to do the integration (Group A, only with EFI data), we removed the quiet time average of E_{xDSL} and E_{yDSL}, calculated E_{zDSL} with offset-removed E_{xDSL} and E_{yDSL}, and then transformed the three components into E_{rGSM}. To avoid systematic errors from the flow velocity or the magnetic field in the cumulative flux transport Φ calculated from the plasma approximation (Groups B–D), we also removed the average $(-\mathbf{v_i} \times \mathbf{B})_y$ of the same time range determined from EFI data from itself. The offset removal procedure may suppress some pre-onset effects, such as the steady increase in Φ due to plasma sheet thinning, tail flapping, or increase/decrease in measured transport caused by balance between convection and inductive tail response to loading. Such effects are hard to diagnose, and are evident in Figures 1c and 1f. The improvement in the superposed epoch analysis application procedure outweighs the disadvantage of suppressing such effects from the above natural or instrumental sources.

[24] Figure 2 shows an example of the offset removal procedure. For Φ obtained with EFI data, it is clear that the offset removal procedure can greatly improve identification of the substorm-related reconnection onset signature (the sudden jump in Φ) without affecting the onset time of that signature (Figures 2c and 2d). Φ calculated from plasma data does not show much difference before and after offset removal (Figures 2g and 2h), because little pre-onset magnetic flux transport was observed in this event.

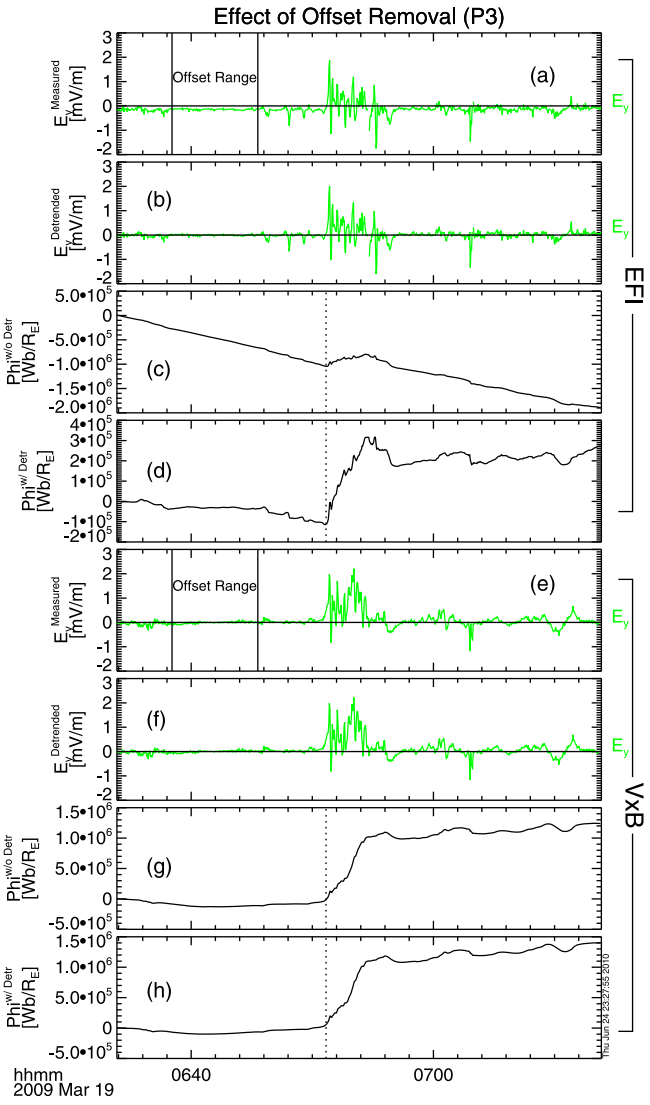

Figure 2. Effect of offset removal. (a) Electric field y component in DSL coordinates (E_{yDSL}) directly measured by the EFI instrument. (b) E_{yDSL} with offset subtracted, the offset determined as the average value in the time range denoted by the two vertical solid lines in Figure 2a. (c) Cumulative flux transport Φ without detrending, i.e., the integration of quantity of Figure 2a over time. (d) Φ with detrending, i.e., the integration of quantity of Figure 2b over time. (e–h) The same quantities in the same order but computed from plasma data ($E = -\mathbf{v_i} \times \mathbf{B}$). The vertical dashed lines denote the onset time of abrupt Φ increases.

[25] After offset removal we integrate E_y (or E_r for Group A; the correct name for the integrated quantities should be E_{y_offset} and E_{r_offset} since the quiet time electric field is obscured, but they are referred to as E_y and E_r hereafter for convenience) to obtain the cumulative magnetic flux transport for each substorm. We superpose all events within each of the four groups with $T = 0$ being the Pi2 onset time of each event (Table 1). The time range shown is $T = -20$ min to $T = 20$ min. Integration is forced to start from $\Phi = 0$ at T = −20 min by subtracting the Φ value at $T = -20$ min from the integral. During various substorm events, different amounts of flux were transported due to varying upstream conditions, and probes made measurements at different downtail distances from the neutral sheet and different Y locations from the substorm meridian. Thus, Φ values vary significantly from observation to observation. When superposing Φ, events with large values overwhelm the results and therefore suppress weaker events. Moreover, when computing Φ from plasma data, we only used the bulk velocity of 0–25 keV (ESA energy range) ions to compute the electric field. This makes the computed electric field smaller than the actual one, which could be improved if the full energy range (using both ESA and SST) of ion contributions to the bulk velocity is considered. We refrain from doing so as performing a case-by-case analysis for each event requires a significant time investment due to calibration issues with the SST data. In addition, the absolute value of the velocity is not critical to the results as long as an increase is observed at the time of reconnection onset. As a result, the Φ calculated from plasma data is often smaller in scale than the one obtained from EFI data for the same observation, even though the two observables follow the same pattern. To properly superpose events from different external geomagnetic conditions, azimuthal and vertical locations, and instruments, we normalized all Φs to their peak value during the superposed time range ($T = -20$ to $T = 20$ min) prior to obtaining their superposed values.

5. Superposed Epoch Analysis: Results

[26] The results of the superposed epoch analysis are shown in Figure 3. For Groups A, C, and D, all the events from Table 1 are used. For Group B, only the events during THEMIS major conjunctions are used because they are enough to produce a statistically significant ensemble. The average and median of the normalized Φs are calculated for each group and plotted at the bottom of Groups A–D.

[27] Figures 3a and 3b show the superposed Φ within 7 R_E downtail and outside the plasmasphere (Group A). Some Φ lines show fluctuations near and immediately after Pi2 onset time. The median and average lines, however, indicate very little Pi2 onset signature, but rather a general trend of increased transport during the active interval. The variability is high partly because few observations were made within 7 R_E down the tail, outside the plasmasphere, and in the premidnight sector, resulting in only 15 observations in this group. Moreover, the probes moved significantly in the inner magnetosphere during the course of 40 min. While the corotational electric field was subtracted from the raw data, the trends may still be affected by the motion of the probes into different L shells during the course of the substorm.

[28] Superposed Φ observations between 7 and 30 R_E (Groups B–D) downtail are presented in Figures 3c–3k. The individual Φ curves obtained from EFI (Figures 3c, 3f, and 3i) are very similar to the ones computed from $-v_i \times B$ (Figures 3d, 3g, and 3j). This similarity is even clearer in the average and median plots (Figures 3e, 3h, and 3k). Note that differences between Figures 3d, 3g, and 3j and Figures 3c, 3f, and 3i do exist: For some events certain probes have EFI data but no ESA data, resulting in fewer

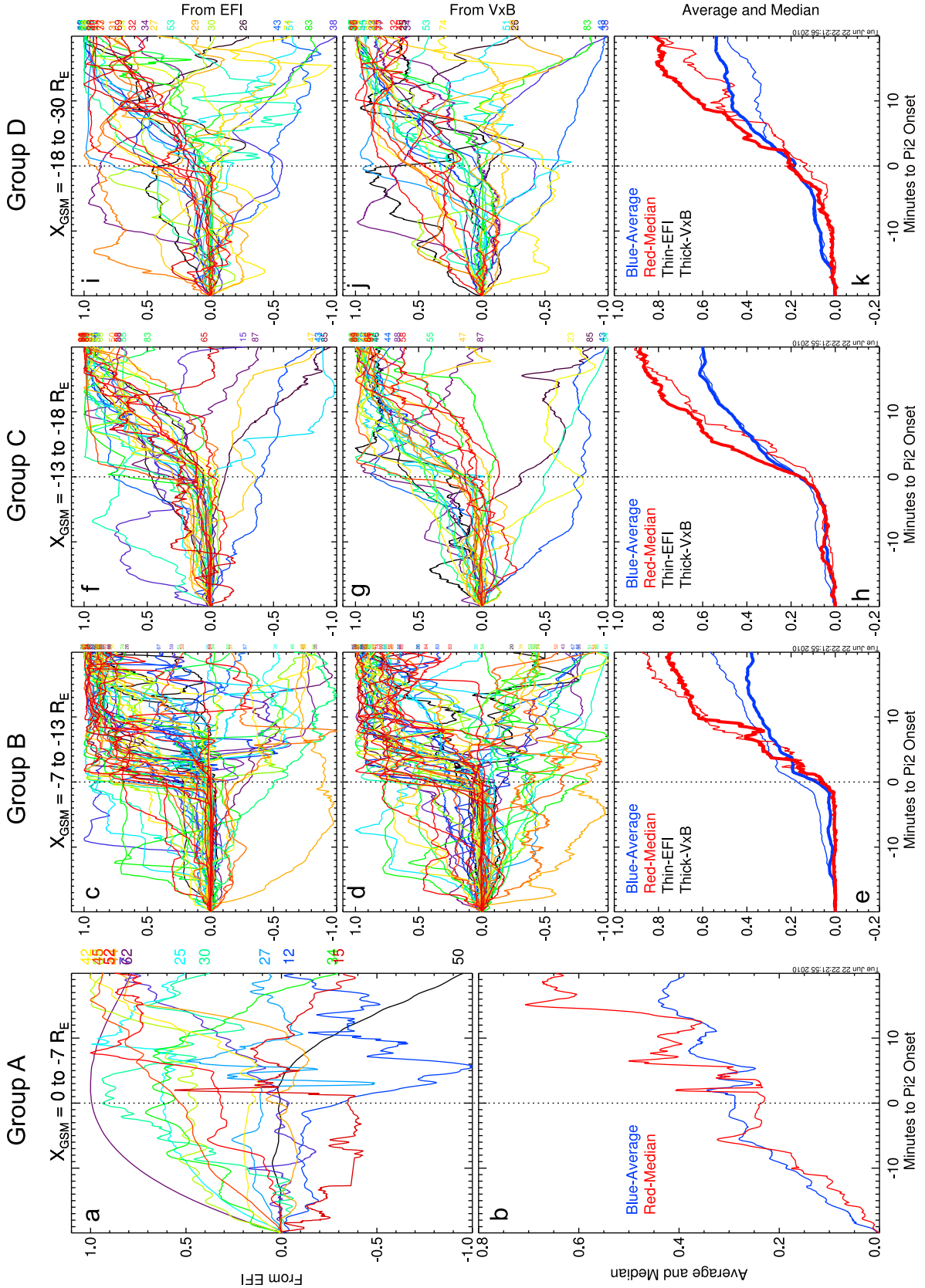
Group A
Group B
Group C
Group D
From EFI
From VxB
Average and Median
Blue-Average
Red-Median
Thin-EFI
Thick-VxB
Minutes to Pi2 Onset

Figure 3

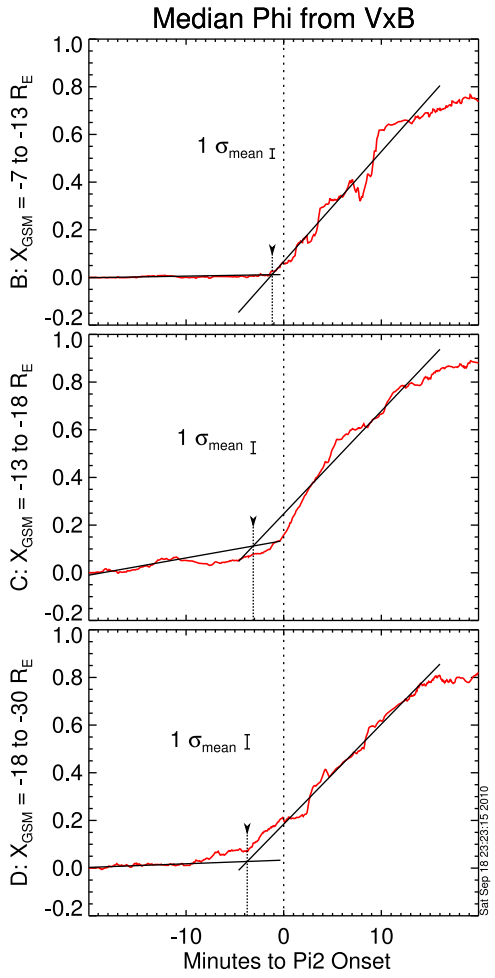

Figure 4. The medians of the superposed normalized cumulative magnetic flux transport Φ computed from plasma data for measurement Groups B–D (red thick lines in Figures 3e, 3h, and 3k). The dotted lines denote the inflection points of the median Φ traces. The inflection point is determined as the cross point of the two thin black lines (linear fit to quiet time and enhancement time; see section 5 for details) in each plot. The σ_{mean} value is the standard deviation of the mean of individual measurements taken at the inflection point.

lines in Figures 3d, 3g, and 3j than in Figures 3c, 3f, and 3i. Additionally, Figures 3d, 3g, and 3j were calculated from GSM, whereas Figures 3c, 3f, and 3i were calculated from DSL E_y. Although individual Φs show slightly different behavior, most suddenly increase near the times of ground Pi2 onsets, as confirmed by their averages and medians in Figures 3e, 3h, and 3k. It is thus clear from Figures 3e, 3h, and 3k that the cumulative magnetic flux transport suddenly jumps a few minutes prior to ground Pi2 onset. The closer the group of measurements to Earth, the more abrupt the increase in cumulative flux transport. The farther the group of measurements from Earth, the larger the noise seen in the ensemble averages or medians. This is partially due to the fact that P3 and P4 (~10 R_E downtail) were much closer to the neutral sheet than P1 and P2 (~15–30 R_E downtail) for our observations, especially for substorm events during the first tail season. Increased distance from the neutral sheet (proximity to the lobe) degrades both electric field observations (in general, lobe EFI measurements have larger offsets and scales than plasma sheet measurements) and plasma observations (in general, particle count rates in the lobes are much smaller than in the plasma sheet). In addition, a small but significant number of events, particularly in Group B, show a monotonic decrease in the flux transport rate. The two major reasons for this population are (1) rebounding flow bursts reported around 10 R_E downtail and accompanied by positive B_z [e.g., *Panov et al.*, 2010] and (2) the tailward parts of vortex structures [e.g., *Keiling et al.*, 2009]. Occasionally, the normalization procedure can result in a spurious monotonically decreasing line. This can happen when an originally smooth line with a very slow decreasing trend (without any significant plasma sheet activations) is normalized by a small pre-onset value and obtains a large slope. The normalization also generates several monotonically increasing lines in each group. On a few other occasions a monotonically decreasing line can be produced by inaccurate, quiet time offset removal. Those spurious lines do not affect the general trends, and were thus left in the database to ensure strict adherence to the stated selection criteria and processing methods.

[29] In the 7–30 R_E data set, the inflection point of the flux rise tends to move closer to $T = 0$ with decreasing distance from Earth. We marked the inflection point using the medians of $-\mathbf{v} \times \mathbf{B}$ in Figure 4. To determine the inflection point more quantitatively, we fit a line to the median trace during the first ten minutes of quiet time (T = −20 to −10 min) and another line to the median trace for 15 min after the zero epoch time (T = 0 to 15 min). The inflection time is then taken as the intersection of these two lines. It is evident that the flux transport start time moves from ~−4 min to ~−1 min as we move from 18–30 R_E to 7–13 R_E downtail. The time delays at different tail locations are interpreted as due mainly to the propagation

Figure 3. Superposed epoch analysis of the normalized cumulative magnetic flux transport Φ measured during the substorm events listed in Table 1. We present the results for measurements in (a and b) Group A, (c–e) Group B, (f–h) Group C, and (i–k) Group D (discussed in section 4). Figures 3a, 3c, 3f, and 3i show the normalized Φ values computed from EFI data (integration of E_{rGSM} for Group A and E_{yDSL} for Groups B–D). Figures 3d, 3g, and 3j show the normalized Φ computed using FGM and ESA data (integration of $(-v_i \times B)_y$). Figures 3b, 3e, 3h, and 3k show the average and median of the traces in Figures 3a, 3c, 3d, 3f, 3g, 3i, and 3j. Note that in Groups B–D, the thin lines are the average and median of the traces in Figures 3c, 3f, and 3i and the thick lines are the average and median of the traces in Figures 3d, 3g, and 3j. Each individual Φ trace is labeled at its right end with a number corresponding to the event observation time, as listed in Table 1 to facilitate independent reproduction and verification of our results.

delay of the substorm activation in X_{GSM} direction, because the azimuthal range of the tail measurements is limited to the Y_{GSM} = 0 to 8 R_E range. Although azimuthal propagation effects may also play a role in this analysis, we consider them secondary for the following reasons. First, if the probe is near the lobes, the flux transport is expected to propagate very quickly (the magnetosonic speed at the lobes is several thousands of km/s depending on the plasma density); thus, time delays would be negligible. Second, the substorm structures are localized in the plasma sheet, so the flux enhancement would have been missed even if the probe was in the plasma sheet but at the wrong azimuthal location.

[30] A final remark is related to the uncertainty of the measurements in the vertical axis. If random noise is causing the trends in the cumulative flux transport, the noise would be uncorrelated with the $T = 0$ line. In our case, however, the fluctuations in the median lines are small, in general far smaller than the rise at $T = 0$. To reinforce that point, we show the representative standard deviation of the mean at the inflection point in each data set in the corresponding plot. The standard deviations of the mean are small relative to the rise in flux transport. However, they are comparable to the variability of the time series of the median at the few minutes surrounding the time of onset. Therefore, the times selected and the trends as functions of distance to Earth are, at this point, suggestive but not completely robust. We anticipate that a larger database of substorms and further event restriction close to the onset meridian will reduce noise and thus improve the statistical significance of these observations.

6. Discussion

[31] We have shown that both EFI and $-\mathbf{v} \times \mathbf{B}$ derived cumulative magnetic flux transport, Φ, observed at all THEMIS probes beyond 7 R_E downtail in the premidnight sector, suddenly increases a few minutes prior to substorm onset as determined by midlatitude Pi2 pulsations. Consistent with previous case studies [*Angelopoulos et al.*, 2009; *Liu et al.*, 2009, 2011], we have demonstrated in a statistical and more general way that Φ can serve as a good indicator for reconnection onset timing at multiple downtail locations.

[32] Our result provides Φ as one more important tail quantity that precedes substorm onset in the near-Earth plasma sheet. We found that the Φ onset time in the 18–30 R_E downtail region precedes midlatitude Pi2 onset on the ground by ~4 min. In general, midlatitude Pi2s are seen 1–2 min after auroral intensification onset. Thus the Φ onset time in the 18–30 R_E downtail region is 2–3 min prior to auroral onset. This is even earlier than the total pressure reduction at 16–20 R_E downtail (2 min prior to auroral onset) found by *Miyashita et al.* [2009] to be the earliest indicator of reconnection.

[33] Early observations of near-Earth convection by *Aggson and Heppner* [1977] showed the presence of large electric field in the inner magnetosphere during the substorm growth phase. Recently *Nishimura et al.* [2009] also found that convective electric field enhancement in the inner magnetosphere has a very small time delay (~5 min) relative to IMF southward turning, whereas electric field enhancement in the outer magnetosphere has a more pronounced delay (~30 min). Our work is consistent with this picture: delayed response in the outer magnetosphere is caused by storage of magnetic flux in the tail and suppression of earthward convection, whereas the onset of the flux transport is likely related to the release of magnetic flux due to tail reconnection. The quick response of the electric field in the inner magnetosphere to the IMF changes may account for the fact that the flux transport measurements in the inner magnetosphere (Group A in Figure 3) are not sorted well by Pi2 timings.

[34] *Nishimura et al.* [2010] demonstrated that the north-south arc starting from PBI precedes premidnight auroral intensification, traditionally defined as substorm onset, by about 5.5 min. *Kepko et al.* [2009] showed the presence of soft electron precipitation in the north-south arc ~2 min prior to a substorm onset, starting 1–2 degrees poleward of the onset arc but within the auroral oval proper. Both north-south arcs from the poleward boundary and from within the oval could potentially be related to near-Earth reconnection and plasmoid formation. Determining how often near-Earth rather than distant tail reconnection is responsible for the avalanche of phenomena leading up to a full-fledged substorm will have to rely on in situ measurements. This paper attempts to establish the robustness of integrated flux transport rate as a signature of reconnection onset and its usage in determining the reconnection onset time. Our findings, pointing to an approximately 4 min delay between tail reconnection onset and Pi2 onset, which (given a 1–2 min delay between Pi2 onset and auroral intensification) suggests a 2–3 min delay between tail reconnection onset and auroral intensifications. Assuming that midtail reconnection proceeds to (or close to) the last closed field line in most of our events, and that the high-speed shear or kinetic Alfvén waves near or along the boundary result in soft auroral acceleration that may be visible as a north-south arc in a small fraction of a minute, the results herein could be viewed as somewhere between the reconnection timing of *Angelopoulos et al.* [2008a] (1.5 min delay), the north-south arc timing of *Kepko et al.* [2009] (2 min delay), and the 5.5 min delay observed by *Nishimura et al.* [2010]. Most of the events in the *Nishimura et al.* [2010] database may have been initiated by near-Earth reconnection but tailward of −30 R_E, which would necessitate a longer coupling time to the inner magnetosphere by earthward flows. This is possible because the THEMIS midtail database was collected in solar minimum, and the anticipated location of the near-Earth reconnection site is known to depend on solar activity [*Nagai et al.*, 2005] moving beyond −25 R_E during solar minimum. This solar cycle bias would affect in situ data but not ground-based data.

[35] We cannot rule out alternate possibilities, however. For example, distant tail reconnection of high-density lobe/mantle plasma 5.5 min prior to onset may result in high-density flows (and north-south arcs). Although these flows could reach only partway to the near-Earth region, they would be close enough to initiate midtail (near-Earth) reconnection ~2 min prior to substorm onset. Reconnection can, in turn, produce low-density flows that, due to their low entropy, are able to protrude deep into the inner edge of the plasma sheet and result in auroral intensification. Alterna-

tively, the distant tail (lobe) reconnection may result in low-density plasma sheet plasma that could result in near-Earth activations.

[36] Testing the consistency of our results further with the aforementioned ground observations for substorm timing and revealing other possible explanations of these results will be the topic of statistical analyses using a more extensive database from THEMIS and the upcoming ARTEMIS mission.

[37] **Acknowledgments.** THEMIS was made possible and is supported in the United States by NASA contract NAS5-02099. Financial support for the FGM instrument was provided by the German Ministry for Economy and Technology and the German Center for Aviation and Space (DLR) under contract 50 OC 0302. We thank the Canadian Space Agency for logistical support in fielding and data retrieval from the GBO stations. CARISMA is operated by the University of Alberta and funded by the Canadian Space Agency. GIMA data are provided by the Geophysical Institute of the University of Alaska Fairbanks, and the Canadian Magnetic Observatory System (CANMOS) network, maintained and operated by the Geological Survey of Canada, also provided data used in this study. The authors are thankful to V. A. Sergeev for useful discussions and his encouragement to build the substorm database. We thank J. Hohl for the help with editing.

References

Aggson, T. L., and J. P. Heppner (1977), Observations of large transient magnetospheric electric fields, *J. Geophys. Res.*, *82*, 5155–5164, doi:10.1029/JA082i032p05155.

Akasofu, S.-I. (1964), The development of the auroral substorm, *Planet. Space Sci.*, *12*, 273–282, doi:10.1016/0032-0633(64)90151-5.

Allan, W., et al. (1996), Are low-latitude Pi2 pulsations cavity/waveguide modes?, *Geophys. Res. Lett.*, *23*, 765–768, doi:10.1029/96GL00661.

Angelopoulos, V. (2008), The THEMIS Mission, *Space Sci. Rev.*, *141*, 5–34, doi:10.1007/s11214-008-9336-1.

Angelopoulos, V., et al. (1992), Bursty bulk flows in the inner central plasma sheet, *J. Geophys. Res.*, *97*, 4027–4039, doi:10.1029/91JA02701.

Angelopoulos, V., et al. (1993), Observations of a quasi-static plasma sheet boundary, *Geophys. Res. Lett.*, *20*, 2813–2816, doi:10.1029/93GL01979.

Angelopoulos, V., et al. (1994), Statistical characteristics of bursty bulk flow events, *J. Geophys. Res.*, *99*, 21,257–21,280, doi:10.1029/94JA01263.

Angelopoulos, V., et al. (2008a), Tail reconnection triggering substorm onset, *Science*, *321*, 931–935, doi:10.1126/science.1160495.

Angelopoulos, V., et al. (2008b), First results from the THEMIS mission, *Space Sci. Rev.*, *141*, 453–476, doi:10.1007/s11214-008-9378-4.

Angelopoulos, V., et al. (2009), Response to comment on "Tail reconnection triggering substorm onset," *Science*, *324*(5933), 1391, doi:10.1126/science.1168045.

Auster, H. U., et al. (2008), The THEMIS Fluxgate Magnetometer, *Space Sci. Rev.*, *141*, 235–264, doi:10.1007/s11214-008-9365-9.

Axford, W. I. (1999), Reconnection, substorms and solar flares, *Phys. Chem. Earth Part C*, *24*(1–3), 147–151, doi:10.1016/S1464-1917(98)00022-1.

Baumjohann, W., and K. Glassmeier (1984), The transient response mechanism and Pi2 pulsations at substorm onset—Review and outlook, *Planet. Space Sci.*, *32*, 1361–1370, doi:10.1016/0032-0633(84)90079-5.

Bonnell, J. W., et al. (2008), The Electric Field Instrument (EFI) for THEMIS, *Space Sci. Rev.*, *141*, 303–341, doi:10.1007/s11214-008-9469-2.

Gabrielse, C., et al. (2009), Timing and localization of near-Earth tail and ionospheric signatures during a substorm onset, *J. Geophys. Res.*, *114*, A00C13, doi:10.1029/2008JA013583.

Gabrielse, C., et al. (2010), Substorm parameter table: An effort to compile signature onset times and values from THEMIS, paper presented at Tenth International Conference on Substorms, Univ. of Calif., San Luis Obispo, Calif.

Hayakawa, H., et al. (1982), Statistical characteristics of plasma flow in the magnetotail, *J. Geophys. Res.*, *87*, 277–283, doi:10.1029/JA087iA01p00277.

Hones, E. W., Jr. (1980), Plasma flow in the magnetotail and its implications for substorm theories, in *Dynamics of the Magnetosphere*, *Astrophys. Space Sci. Libr.*, vol. 78, edited by S.-I. Akasofu, pp. 545–562, D. Reidel, Dordrecht, Netherlands.

Jacobs, J. A., et al. (1964), Classification of geomagnetic micropulsations, *J. Geophys. Res.*, *69*, 180–181, doi:10.1029/JZ069i001p00180.

Keiling, A., et al. (2009), Substorm current wedge driven by plasma flow vortices: THEMIS observations, *J. Geophys. Res.*, *114*, A00C22, doi:10.1029/2009JA014114.

Kepko, L., and R. L. McPherron (2001), Comment on "Evaluation of low-latitude Pi2 pulsations as indicators of substorm onset using Polar ultraviolet imagery" by K. Liou et al., *J. Geophys. Res.*, *106*, 18,919–18,922, doi:10.1029/2000JA000189.

Kepko, L., et al. (2002), ULF waves in the solar wind as direct drivers of magnetospheric pulsations, *Geophys. Res. Lett.*, *29*(8), 1197, doi:10.1029/2001GL014405.

Kepko, L., et al. (2009), Equatorward moving auroral signatures of a flow burst observed prior to auroral onset, *Geophys. Res. Lett.*, *36*, L24104, doi:10.1029/2009GL041476.

Liou, K., et al. (2000), Evaluation of low-latitude Pi2 pulsations as indicators of substorm onset using Polar ultraviolet imagery, *J. Geophys. Res.*, *105*, 2495–2506, doi:10.1029/1999JA900416.

Liu, J., et al. (2009), THEMIS observation of a substorm event on 04:35, 22 February 2008, *Ann. Geophys.*, *27*, 1831–1841, doi:10.5194/angeo-27-1831-2009.

Liu, J., et al. (2011), Revised timing and onset location of two isolated substorms observed by Time History of Events and Macroscale Interactions During Substorms (THEMIS), *J. Geophys. Res.*, *116*, A00I17, doi:10.1029/2010JA015877.

Lopez, R. E., and A. T. Y. Lui (1990), A multisatellite case study of the expansion of a substorm current wedge in the near-Earth magnetotail, *J. Geophys. Res.*, *95*, 8009–8017, doi:10.1029/JA095iA06p08009.

Lyons, L. R., et al. (2010a), Substorm triggering by new plasma intrusion: Incoherent-scatter radar observations, *J. Geophys. Res.*, *115*, A07223, doi:10.1029/2009JA015168.

Lyons, L. R., et al. (2010b), Enhanced transport across entire length of plasma sheet boundary field lines leading to substorm onset, *J. Geophys. Res.*, *115*, A00I07, doi:10.1029/2010JA015831.

Mann, I. R., et al. (2008), The upgraded CARISMA magnetometer array in the THEMIS era, *Space Sci. Rev.*, *141*, 413–451, doi:10.1007/s11214-008-9457-6.

McFadden, J. P., et al. (2008), THEMIS ESA first science results and performance issues, *Space Sci. Rev.*, *141*, 477–508, doi:10.1007/s11214-008-9433-1.

McPherron, R. L. (1979), Magnetospheric substorms, *Rev. Geophys. Space Phys.*, *17*, 657–681, doi:10.1029/RG017i004p00657.

McPherron, R. L., et al. (1973), Substorms in space: The correlation between ground and satellite observations of the magnetic field, *Radio Sci.*, *8*, 1059–1076, doi:10.1029/RS008i011p01059.

Mende, S. B., et al. (2003), FAST and IMAGE-FUV observations of a substorm onset, *J. Geophys. Res.*, *108*(A9), 1344, doi:10.1029/2002JA009787.

Mende, S. B., et al. (2008), The THEMIS array of ground-based observatories for the study of auroral substorms, *Space Sci. Rev.*, *141*, 357–387, doi:10.1007/s11214-008-9380-x.

Miyashita, Y., et al. (2009), A state-of-the-art picture of substorm-associated evolution of the near-Earth magnetotail obtained from superposed epoch analysis, *J. Geophys. Res.*, *114*, A01211, doi:10.1029/2008JA013225.

Nagai, T. (2006), Location of magnetic reconnection in the magnetotail, *Space Sci. Rev.*, *122*, 39–54, doi:10.1007/s11214-006-6216-4.

Nagai, T., et al. (1998), Structure and dynamics of magnetic reconnection for substorm onsets with Geotail observations, *J. Geophys. Res.*, *103*, 4419–4440, doi:10.1029/97JA02190.

Nagai, T., et al. (2005), Solar wind control of the radial distance of the magnetic reconnection site in the magnetotail, *J. Geophys. Res.*, *110*, A09208, doi:10.1029/2005JA011207.

Nishida, A., et al. (1981), Observed signatures of reconnection in the magnetotail, *J. Geophys. Res.*, *86*, 1422–1436, doi:10.1029/JA086iA03p01422.

Nishimura, Y., et al. (2009), Response of convection electric fields in the magnetosphere to IMF orientation change, *J. Geophys. Res.*, *114*, A09206, doi:10.1029/2009JA014277.

Nishimura, Y., et al. (2010), Substorm triggering by new plasma intrusion: THEMIS all-sky imager observations, *J. Geophys. Res.*, *115*, A07222, doi:10.1029/2009JA015166.

Panov, E. V., et al. (2010), Multiple overshoot and rebound of a bursty bulk flow, *Geophys. Res. Lett.*, *37*, L08103, doi:10.1029/2009GL041971.

Pritchett, P. L., and F. V. Coroniti (1995), Formation of thin current sheets during plasma sheet convection, *J. Geophys. Res.*, *100*, 23,551–23,565, doi:10.1029/95JA02540.

Pu, Z. Y., et al. (2010), THEMIS observations of substorms on 26 February 2008 initiated by magnetotail reconnection, *J. Geophys. Res.*, *115*, A02212, doi:10.1029/2009JA014217.

Russell, C. T., et al. (2008), THEMIS ground-based magnetometers, *Space Sci. Rev.*, *141*, 389–412, doi:10.1007/s11214-008-9337-0.

Saito, T. (1969), Geomagnetic pulsations, *Space Sci. Rev.*, *10*, 319–412, doi:10.1007/BF00203620.

Sergeev, V. A., et al. (2000), Multiple-spacecraft observation of a narrow transient plasma jet in the Earth's plasma sheet, *Geophys. Res. Lett.*, *27*, 851–854, doi:10.1029/1999GL010729.

Sibeck, D. G., and V. Angelopoulos (2008), THEMIS science objectives and mission phases, *Space Sci. Rev.*, *141*, 35–59, doi:10.1007/s11214-008-9393-5.

Slavin, J. A., et al. (1984), Substorm associated traveling compression regions in the distant tail: ISEE-3 Geotail observations, *Geophys. Res. Lett.*, *11*, 657–660, doi:10.1029/GL011i007p00657.

Takahashi, K., et al. (2003), CRRES electric field study of the radial mode structure of Pi2 pulsations, *J. Geophys. Res.*, *108*(A5), 1210, doi:10.1029/2002JA009761.

Zesta, E., et al. (2000), The auroral signature of earthward flow bursts observed in the magnetotail, *Geophys. Res. Lett.*, *27*, 3241–3244, doi:10.1029/2000GL000027.

V. Angelopoulos, C. Gabrielse, and J. Liu, IGPP, ESS, University of California, Los Angeles, CA 90095-1567, USA. (jliu@igpp.ucla.edu)

J. Bonnell and J. P. McFadden, Space Sciences Laboratory, University of California, 7 Gauss Way, Berkeley, CA 94720-7450, USA.

N. A. Frissell, Bradley Department of Electrical and Computer Engineering, Virginia Polytechnic Institute and State University, 1991 Kraft Dr., Ste. 2019, Blacksburg, VA 24060, USA.

K. H. Glassmeier, Technische Universität Braunschweig, D-38106 Braunschweig, Germany.

L. R. Lyons, Department of Atmospheric and Oceanic Sciences, University of California, 405 Hilgard Ave., Los Angeles, CA 90095-1565, USA.